Matter and Radiation at Extremes | RESEARCH ARTICLE | scitation.org/journal/mre

Static and dynamic diamond anvil cell (s-dDAC): A bidirectional remote controlled device for static and dynamic compression/decompression

Cite as: Matter Radiat. Extremes 7, 018401 (2022); doi: 10.1063/5.0061583
Submitted: 28 June 2021 • Accepted: 12 November 2021 •
Published Online: 14 December 2021

Lei Su,[1,2,a] Kaiyuan Shi,[2] Li Zhang,[1] Yanlong Wang,[2] and Guoqiang Yang[1,a]

AFFILIATIONS

[1]Key Laboratory of Photochemistry, Institute of Chemistry, University of Chinese Academy of Sciences, Chinese Academy of Sciences, Beijing 100190, China
[2]Center for High Pressure Science and Technology Advanced Research, Beijing 100094, China

[a]**Authors to whom correspondence should be addressed:** leisu2050@iccas.ac.cn and gqyang@iccas.ac.cn

ABSTRACT

A novel bidirectional remotely controlled device for static and dynamic compression/decompression using diamond anvil cells (DACs) has been developed that can control pressure in an accurate and consistent manner. Electromechanical piezoelectric actuators are applied to a conventional DAC, allowing applications under a variety of pressure conditions. Using this static and dynamic DAC (s-dDAC), it is possible to addresses the poorly studied experimental regime lying between purely static and purely dynamic studies. The s-dDAC, driven by three piezoelectric actuators, can be combined with a time-resolved spectral measurement system and high-speed imaging device to study the structural changes, chemical reactions, and properties of materials under extreme conditions. The maximum compression/decompression rate or pressure range highly depends on the culet size of the anvil, and a higher compression rate and wider pressure range can be realized in a DAC with smaller anvil culet. With our s-dDAC, we have been able to achieve the highest compression rate to date with a 300 μm culet anvil: 48 TPa/s. An overview of a variety of experimental measurements possible with our device is presented.

I. INTRODUCTION

High-pressure experimental techniques have conventionally been classified as adopting one of two different approaches: static high pressure and dynamic high pressure. From the perspective of heat conduction, if the loading process of the system is fast enough, and there is no exchange heat with the outside; such a process is called an adiabatic process. If the loading process is sufficiently slow that heat exchange is possible and the system is always in thermal balance with its surroundings, then such a process is called isothermal. In general, dynamic high-pressure experiments are considered to be adiabatic because of the rapid pressurization that is used, while static high-pressure experiments are considered to be isothermal because of the slow pressurization.[1] In fact, however, there is another approach to pressure loading/unloading that is exemplified by the static and dynamic diamond anvil cell (s-dDAC) considered in this paper, for which the pressurization rate is higher than that of the static high-pressure technique and lower than that of the dynamic high-pressure technique. Thus, the physical process involved is neither isothermal nor adiabatic, but a special intermediate process. The aim of this approach is to bridge the gap between static and dynamic experiments and address issues regarding the kinetics of transformations at high pressures.[2]

Over the last few years, considerable effort has been devoted to the development of instrumentation for remote and automated pressure control.[3–9] One such device is the dynamic diamond anvil cell (dDAC), which repetitively applies a time-dependent load/pressure profile to a sample. It was developed in 2007 by Evans *et al.*,[10] and has played perhaps the most important role in recent high-pressure research, with many important applications in physics, chemistry, materials science, geonomy, and biosciences. The dDAC allows studies of the kinetics of phase transitions and the evolution of metastable phases at compression rates up to 500 GPa/s.[10,11] Yoo and co-workers[12,13] used a dDAC to study the pressure-induced crystal growth of ice and high-density amorphous ice at room temperature. Research teams at the Advanced Photon Source (APS) in the USA and the Petra III synchrotron radiation light source in Germany combined time-resolved x-ray diffraction (XRD) with the

dDAC technique[14–16] and studied the metastable phases of Bi, H_2O, Ge, and other substances in detail.[17–21] Li and co-workers, from the Institute of High Energy Physics of the Chinese Academy of Sciences, developed a dDAC technique at the Beijing Synchrotron Radiation Source and studied the kinetics of phase transitions and the evolution of metastable phases using symmetric DACs.[22] Sun and co-workers developed a piezoelectrically driven dDAC device that was able to achieve continuous *in situ* tuning of high pressures at temperatures as low as 20 K. They applied this device to the measurement of low-temperature pressure-dependent spectra of single quantum dots and two-dimensional layered materials.[23–26]

To further develop these experimental techniques, a bidirectional remote control device for static and dynamic compression/decompression using DACs has been developed. With the static and dynamic diamond anvil cell (s-dDAC), it is possible to remotely control pressure in an accurate and consistent manner by using electromechanical actuators to apply a load, producing a tailored time-dependent pressure profile on a sample. The major advantages of the s-dDAC system are that it allows effective pressure changes with ultrahigh pressure and spatio-temporal resolutions, it can be combined with equipment for time-resolved spectroscopy, and it has a large lateral space available, which is conducive to the development of electrical and heating experiments. It is thus an effective instrument for exploring fundamental problems in physics, chemistry, materials science, earth sciences, and biology under extreme conditions.

II. EXPERIMENTS

A. Design of the s-dDAC device

The s-dDAC is designed to allow precise pressure control through the use of piezoelectric actuators. Figure 1 presents schematic representations of the device, together with a photograph showing its detailed structure, in which two DACs are assembled to the left and right of a central pressure plate for compression and decompression, respectively. The s-dDAC is made of type 440c stainless steel except for the DACs and piezoelectric actuators, and the complete assembly weight is about 8.5 kg. Such a device structure is compatible with various types of DACs, for instance, in the device described here, DAC 1 is a guide pillar type and DAC 2 is a piston–cylinder type. Three piezoelectric actuators (Nanomotions, Model PAL40VS25) are symmetrically fixed on the cylindrical main frame, and the central pressure plate is placed at the end of the three piezoelectric actuators for uniform pressure loading. These piezoelectric actuators can expand by 38 μm with a wide input voltage of 150 V and together generate a maximum push force of ~22 kN. DAC 1 is used in compression mode, avoiding contact between the DAC screws and the pressure plate, and a single short cylinder is used that can be replaced according to DAC type. The left preloading screw clamps DAC 1 and applies precompression. When the voltage on the three piezoelectric actuators is increased, they expand and apply an expansive load to DAC 1. Conversely, in decompression mode, DAC 2 is first precompressed through the four screws in the cell body and then tightly fixed between the pressure plate and the right preloading screw. Finally, the expansion of the piezoelectric actuators separates the two parts of the DAC and decreases the pressure. To enable *in situ* detection of sample signals, all the main components of the s-dDAC possess optical apertures, including the preloading screw, cylinder, and pressure plate. Furthermore, benefitting from the open design of the main frame, quite a bit of room is left for complex DAC experiments, such as electrical measurements, radial diffraction measurements, and resistive heating experiments.

B. Operational details

A function generator (Gwinstek, Type AFG-3051) is utilized to precisely control the displacement of the piezoelectric actuator and

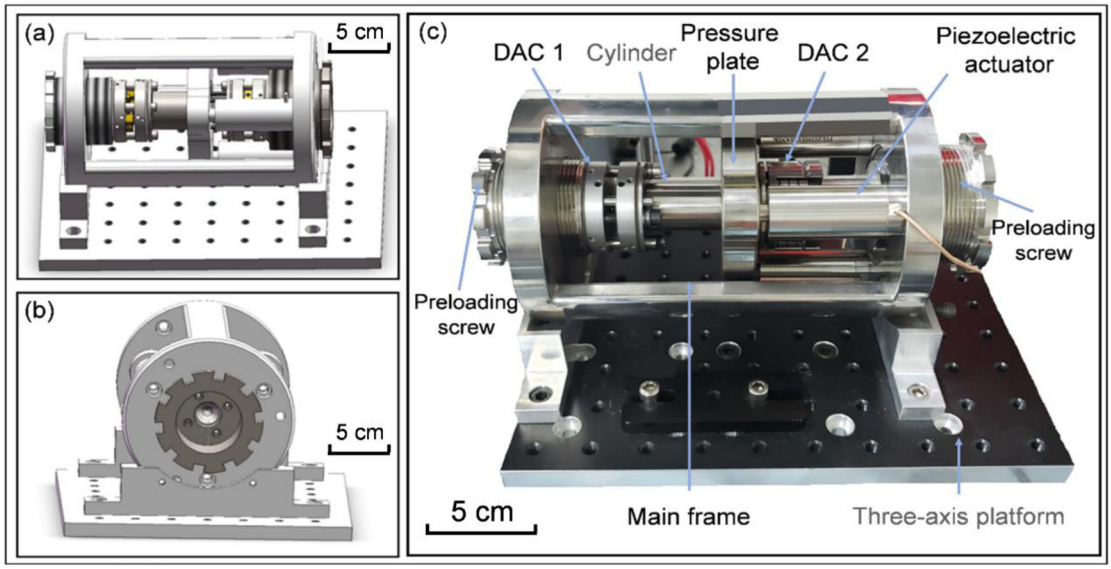

FIG. 1. The s-dDAC assembled with two DACs for compression and decompression: (a) schematic front view; (b) schematic side view; (c) photograph and details of the components.

realize the dynamic pressure load. As illustrated in Fig. 2, the generated waveform (0–5 V) synchronously controls three piezoelectric amplifiers/power supplies (same type) and applies a voltage of 0–150 V to the piezoelectric actuators. Meanwhile, the function generator sends trigger signals to two optical detectors to measure the sample's signal and a ruby fluorescence signal (pressure gauge). Periodic waveforms, such as triangular, trapezoidal, sinusoidal, and other customized functions, drive the repeated compression–decompression cycles of the DAC within the elastic deformation region of the gasket. The compression/decompression rate can be altered easily by changing the slope of the ramp waveform. It is obvious that through modulation of the output magnitude, frequency, and waveform of the arbitrary function generator, the range and rate of the pressure changes can be finely and continuously adjusted—hence the name static and dynamic DAC.

As mentioned above, the s-dDAC device exhibits outstanding performance in static and dynamic pressure loading. The compression/decompression process can induce a wealth of structural transformations and lead to dramatic changes in material properties. However, the s-dDAC technique has not been widely used in experiments, and few suitable *in situ* time-resolved detection methods are available in the high-pressure laboratory. We have therefore designed a versatile time-resolved spectral (fluorescence, Raman, and UV–visible absorption) and high-speed imaging system for the s-dDAC (Fig. 3). This system is set up on an optical table with an area of $1.8 \times 2.4\ m^2$. The s-dDAC is fixed to a three-axis electrically driven moving platform, and the imaging system is adapted from a Leica microscope (Type DM2700). A xenon lamp located behind the s-dDAC is used as the light source for back illumination and UV–visible absorption. Four lasers with different wavelengths are installed in this system. The 375 and 405 nm lasers are used for fluorescence spectroscopy and the 532 and 785 nm lasers for Raman measurements. The laser light path can be altered through a laser switch box with a push–pull structure. Four groups of optical filters are integrated on a high-precision electrically driven rotary carrier, and the optical light paths can be switched automatically. A 677 nm single-edge dichroic beam splitter is installed to separate the sample signal and ruby fluorescence (R1 peak, 694.2 nm under ambient conditions). Two intensified charge-coupled devices (ICCDs, Andor, DH334T) of the same type are assembled in two of the same spectrometers with a 500 mm focal length (Andor, SR500i), and each spectrometer has three gratings (150 grooves/mm, 600 grooves/mm, and 1200 grooves/mm) to meet different spectral needs. This ICCD

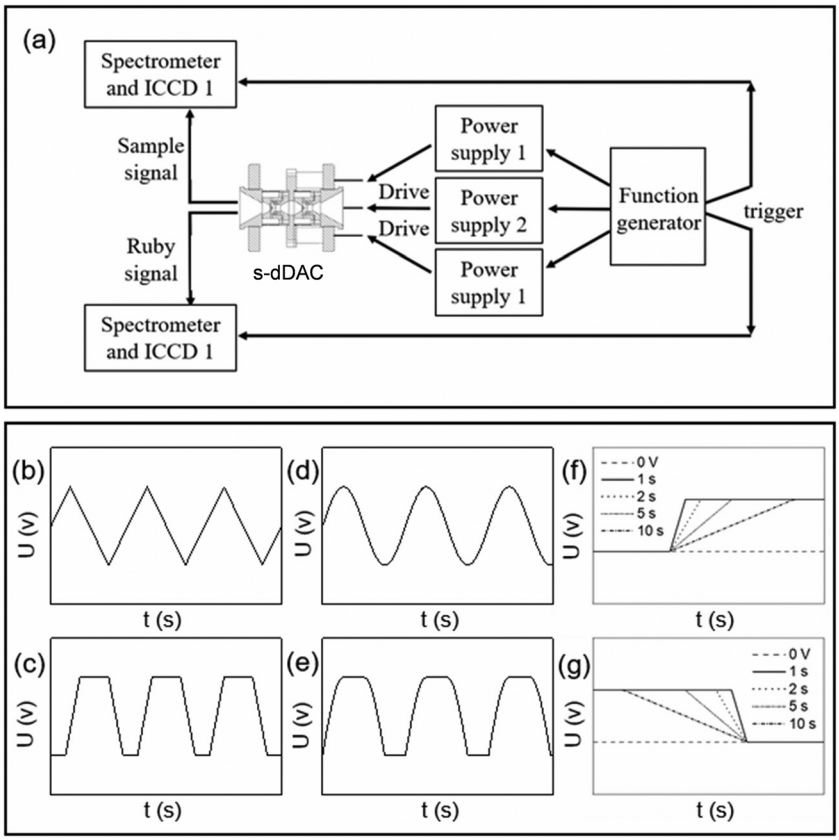

FIG. 2. Control of the dynamic pressure load of the s-dDAC by the function generator. (a) Schematic of s-dDAC operation and spectral detection. (b)–(e) Periodic waveforms (triangular, trapezoidal, sinusoidal, and customized functions) from the function generator for repeated compression/decompression cycles of the DAC. (f) and (g) Ramp waveforms for different compression and decompression rates.

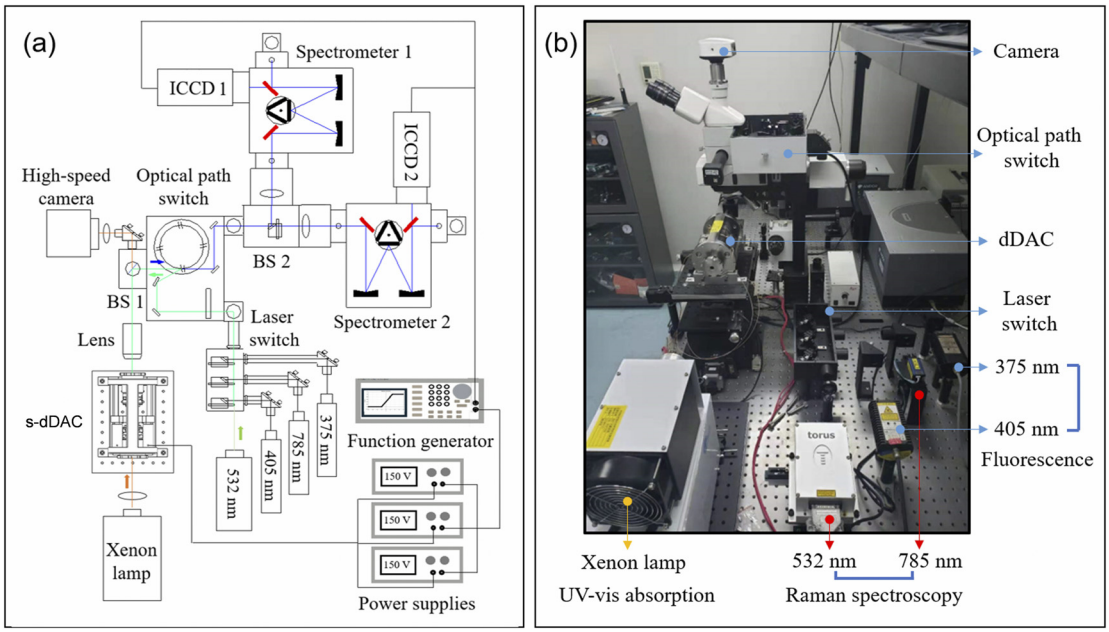

FIG. 3. (a) Schematic (a) and (b) photograph of the versatile time-resolved fluorescence/Raman/UV-visible absorption spectroscopy and high-speed imaging system.

detector allows continuous collection of spectral signals with an exposure time of 100 μs. Thus, the sample signal and ruby fluorescence can be separately detected by two detectors. Furthermore, a high-speed camera (Pco. dimax cs4, 2016 × 2016 resolution, 1102 frames/s) is used to observe the color, luminescence, morphology, and nucleation growth of a sample during rapid compression/decompression, and the frame rate can be raised to more than 10 000 frames/s, although at the price of decreased resolution. Overall, this versatile time-resolved (>100 μs) fluorescence/Raman/UV–visible absorption spectral detection and high-speed imaging system is a powerful tool for investigating structural transformations and optical property changes during dynamic pressure loading.

A complete pressure drive involves the coordinated action of several different piezoelectric actuators and power supplies. Poor synchronization between these components will drag down the response rate and decrease the compression pressure, and can even damage the brittle piezoelectric actuators. As shown in Figs. 4(a) and 4(b), the output voltages of the three power supplies driven by a square waveform and a ramp waveform, respectively, were collected by an oscilloscope. The output curves perfectly overlap each other, even on a microsecond scale, indicating high synchronization among these power supplies. The shortest response time of the s-dDAC was measured by driving it with a burst signal. The s-dDAC was pre-compressed to 5 GPa and rapidly pressurized to 29 GPa within 0.5 ms (a compression rate of 48 TPa/s, with a 300 μm culet anvil), demonstrating its quick response time [Fig. 4(c)]. Then, the s-dDAC was compressed under a ramp compression in 20 ms and in 100 ms. The results indicate that the s-dDAC was able to accurately control the compression rate [Fig. 4(d)]. It should be mentioned that the maximum compression rate or pressure range depends strongly on the culet size of the anvil: a higher compression rate and wider pressure range can be realized in a DAC with a smaller anvil culet. The 48 TPa/s in our experiment is the highest compression rate yet achieved in a DAC with a 300 μm culet anvil. Owing to the trigger control between the s-dDAC and the two detectors, simultaneous collection of the sample signal and the ruby fluorescence in a single compression process is also possible. As shown in Figs. 4(e) and 4(f), an organic molecular crystal was pressurized with ramp compression, and the time-resolved spectra of the sample and ruby correspond, based on the timestamp.

III. APPLICATIONS

A. Compression-rate-dependent crystallization of materials

The polymorphism of materials under high pressure has attracted great attention. As one of the simplest aromatic compounds, pyridine (C_5H_5N) has a rich crystalline phase under high pressure. However, how to obtain specific crystalline phases remains controversial, and completely opposite results have even been obtained. Here, we investigate in depth the crystallization of pyridine under various compression rates. Figure 5 shows optical images and XRD patterns obtained during the compression of initially liquid pyridine up to 1.20 GPa and its crystallization at the same input voltage and different compression times. From the time-resolved optical images in Figs. 5(a) and 5(b), it can be seen that the compression rate has an effect on the initial crystallization pressure, resulting in different crystal morphologies. The XRD patterns confirm that these two crystals are phase III [Fig. 5(c)] and phase I [Fig. 5(d)], respectively. Thus, on rapid compression from 0.3 to ~1.20 GPa, pyridine crystallizes to phase III, but with slow compression, it crystallizes to phase I. These results demonstrate that the compression rate can be used to

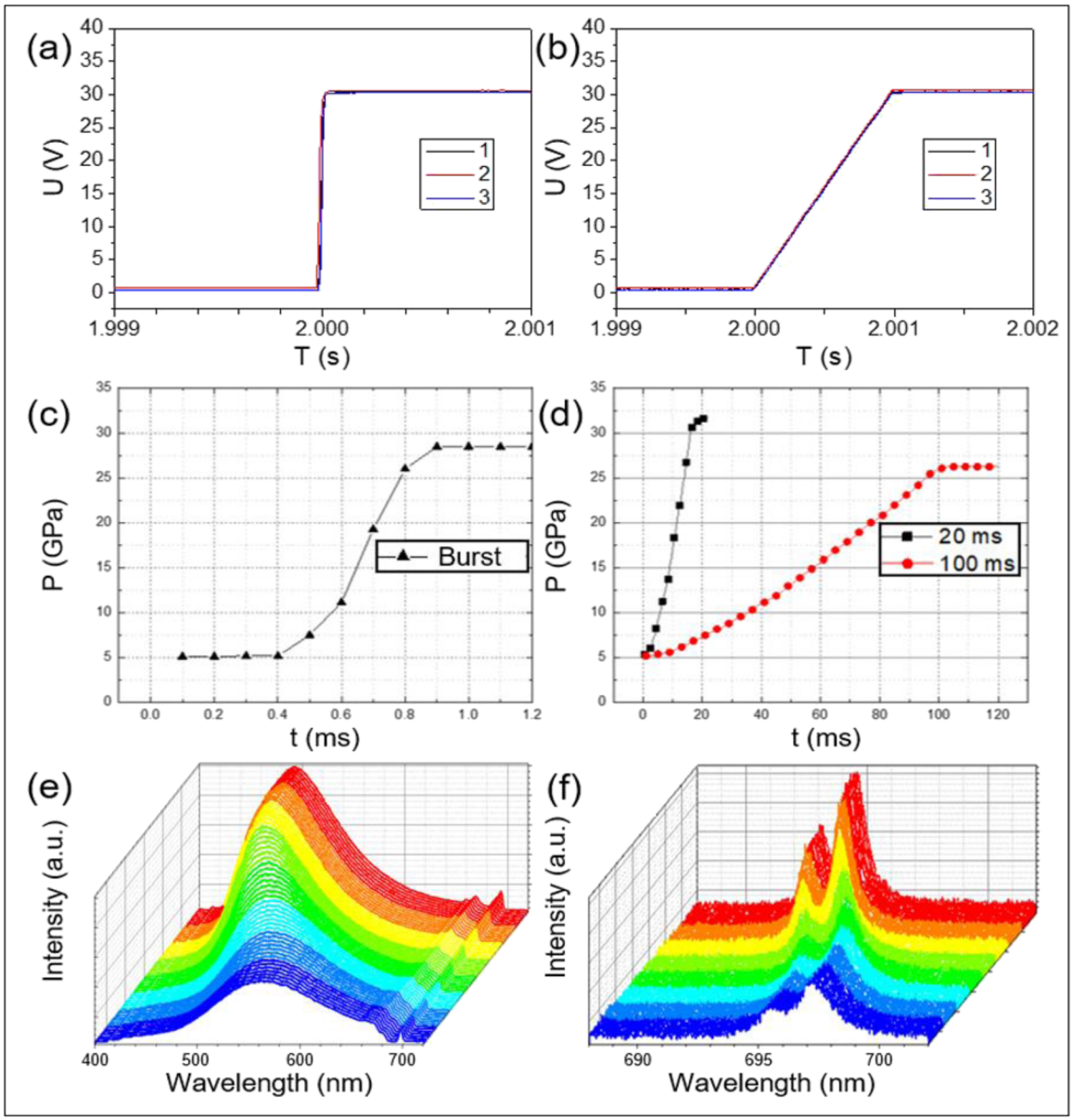

FIG. 4. The dynamic pressure drive of the s-dDAC is controlled by the function generator. (a) and (b) Output voltages of the three power supplies driven by a square waveform and a ramp waveform, respectively. (c) Compression of the s-dDAC from 5 to 29 GPa within 0.5 ms under a burst signal drive. (d) Compression of the s-dDAC in 20 ms and in100 ms under a ramp waveform drive. (e) and (f) Evolution of sample fluorescence and ruby fluorescence in a single compression process.

selectively control the nucleation pathway to obtain different target products, which will contribute to a better understanding of the crystallization kinetics of materials under high pressure.[27]

B. Characterization of the mechanoluminescence process

Mechanoluminescence (ML) is an intriguing light emission phenomenon that has a wide range of applications in stress sensing,[28] anti-counterfeiting,[29] and novel light sources and displays.[30] ML is a highly time- and space-dependent dynamic process that emits light with weak intensity and transient properties, and consequently it is a challenging task to accurately and completely detect, characterize, and describe the process with high resolution.[31] The s-dDAC and its *in situ* spectral characterization system described in this article are particularly suitable for studies of ML. It can achieve high-resolution spectral collection under dynamic compression and greatly expand the pressure range of ML research to the GPa level, which is

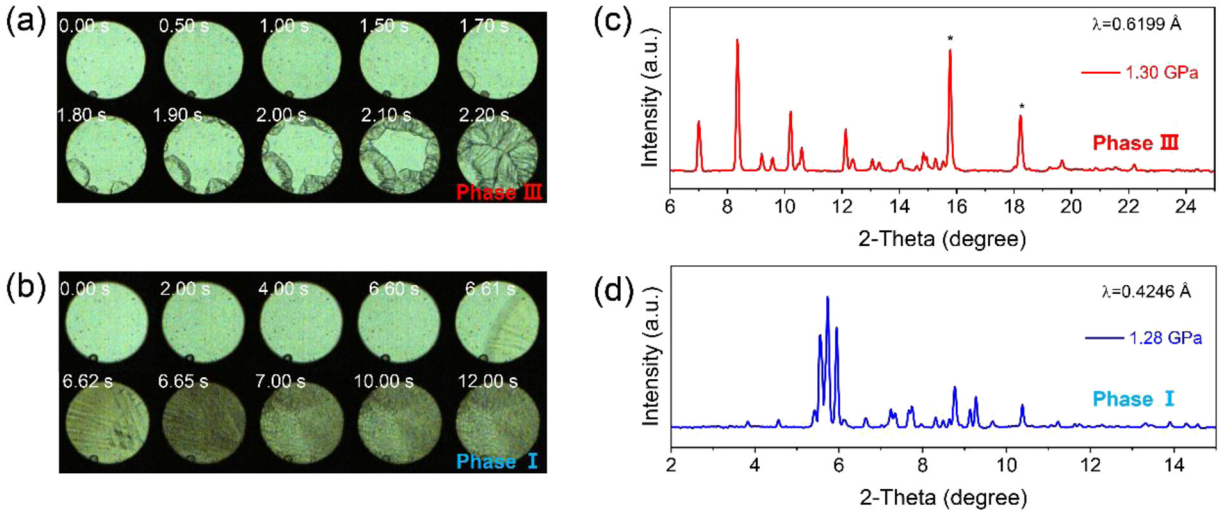

FIG. 5. (a) and (b) Selected time-resolved optical images of liquid pyridine with compression times of 1 and 10 s, respectively. (c) and (d) XRD patterns of pyridine at 1.30 GPa with a compression time of 1 s and at 1.28 GPa with a compression time of 10 s, respectively.

inaccessible using other apparatus. This technique provides a platform for characterizing the behavior of ML materials and provides the possibility of understanding the mechanism of ML. Taking manganese-doped zinc sulfide (ZnS:Mn) as an example, we studied its ML using the s-dDAC device. ZnS:Mn samples were sealed in the s-dDAC at 1.1 GPa and compressed to 7.3 GPa in 1 s with a 6.2 GPa/s compression rate. Interestingly, with increasing pressure, the intensity of ML first increases and then decreases, accompanied by a spectral redshift (~45 nm) [Figs. 6(a) and 6(b)]. This is the first time that a continuous red shift of the ML spectrum has been observed with changes in pressure. Furthermore, the good linear relationship between the ML peak position and pressure makes it possible for this to be used as a pressure gauge without external excitation during the dynamic compression process.

From the pressure dependence of the ML intensity of ZnS:Mn during dynamic compression in the GPa range (Fig. 6), together with

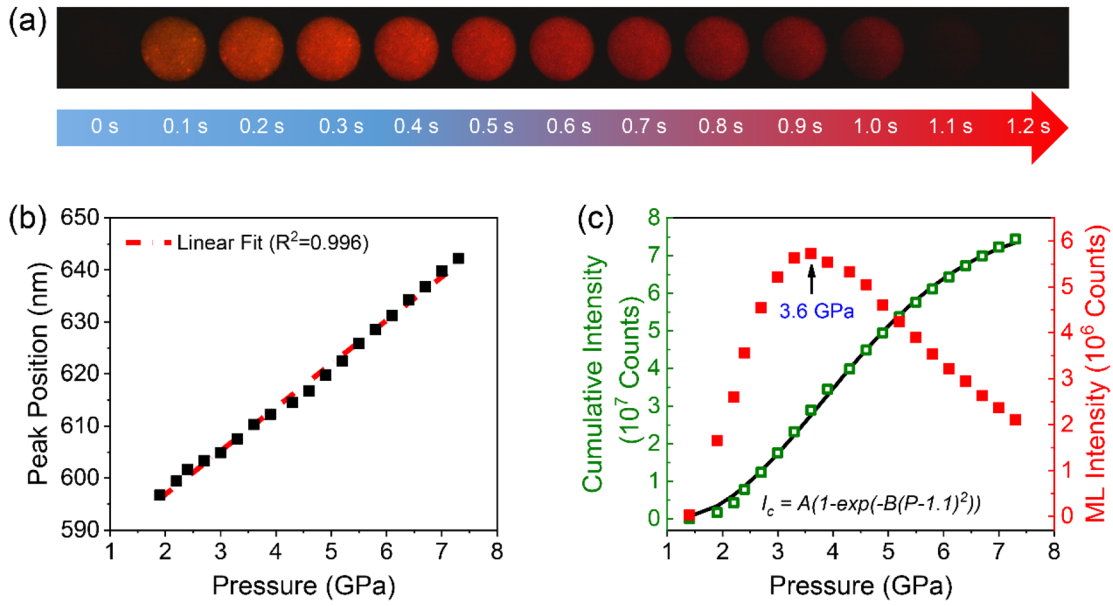

FIG. 6. ML process of ZnS:Mn compressed from 1.1 to 7.3 GPa in 1 s. (a) Selected time-resolved images of ZnS:Mn. (b) Relationship between pressure and ML peak position of ZnS:Mn. (c) Relationship between ML intensity, cumulative intensity, and pressure.

the results of theoretical analysis, the modulating and optimizing effects of the introduction of surface defects on the electronic structure can be demonstrated. The interlayer structure of ZnS:Mn under high pressure is closely related both to the applied compression and to the presence of vacancies. These play opposite roles in luminescence, and thus their combined effect leads to a hill-shaped trend in ML intensity. This offers a novel strategy for the color tuning of luminescent materials, as well as a promising way to explore the mechanism of ML.[32,33]

IV. CONCLUSIONS AND OUTLOOK

To overcome some of the disadvantages of current DAC techniques, a bidirectional remotely controlled device for static and dynamic compression/decompression has been developed. This static and dynamic DAC (s-dDAC) device comprises two DACs, which are held on the left and right parts, respectively, of a fixed frame by two static pressure screws passing through threaded holes. The device can load/unload both DACs at the same time, and the loading/unloading method is simple and highly efficient, greatly improving the ability to carry out high-pressure experiments.

The device can also be used for conducting experiments involving the loading/unloading of a single DAC. In this configuration, the DAC sits in a groove on the upper surface of the pressure plate and is held by a static pressure screw passing through a threaded hole in the left part of the fixed frame. In an alternative arrangement, the DAC sits in a groove on the lower surface of the pressure plate and the static pressure screw holds it through a threaded hole in the right part of the fixed frame.

The device can be used with a variety of types of DAC, including among others, symmetrical DACs and guide pillar DACs. It has a large operating space around it, which makes it compatible with equipment for high-voltage electrical testing and for providing high-temperature and high-pressure environments. This also allows experimenters to observe the status of the DAC during operation. The device can be used in conjunction with *in situ* Raman spectrometers, fluorescence spectrometers, absorption spectrometers, and high-speed imaging equipment, as well as with synchrotron radiation light sources. Moreover, a lateral opening DAC can be installed to enable radial x-ray line studies.

The s-dDAC has a large pressurization rate and a measurable pressure range that represent a breakthrough in high-pressure research. The compression/decompression process associated with this device is neither isothermal nor adiabatic, but a special intermediate type, and it enables the study of a variety of structural transformations. Use of the s-dDAC is expected to lead to significant research results in a number of areas of chemistry, physics, biology, materials science, and other disciplines, including for example, the preparation of metastable-phase materials, the study of phase change kinetics, and ultra-high-pressure chemical synthesis.

ACKNOWLEDGMENTS

This work is supported by the National Natural Science Foundation of China (Grant No. 21627802) and the Strategic Priority Research Program of Chinese Academy of Sciences (Grant No. XDB17000000).

AUTHOR DECLARATIONS

Conflict of Interest

The authors have no conflicts to disclose.

DATA AVAILABILITY

Some or all data, models, or code generated or used during the study are available from the corresponding author by request.

REFERENCES

[1]S. M. Hong, L. Y. Chen, X. R. Liu *et al.*, "High pressure jump apparatus for measuring Grűneisen parameter of NaCl and studying metastable amorphous phase of poly (ethylene terephthalate)," Rev. Sci. Instrum. **76**, 053905 (2005).

[2]C. L. Lin and J. S. Tse, "High-pressure nonequilibrium dynamics on second-to-microsecond time scales: Application of time-resolved X-ray diffraction and dynamic compression in ice," J. Phys. Chem. Lett. **12**, 8024–8038 (2021).

[3]J. Quednau and G. M. Schneider, "A new high-pressure cell for differential pressure-jump experiments using optical detection," Rev. Sci. Instrum. **60**, 3685–3687 (1989).

[4]S. Sinanis and G. M. Schneider, "Pressure-jump investigations on the kinetics of the isotropic-nematic phase transition of a liquid crystal: Time behavior of the scattered and transmitted light intensities for PCH 5," Ber. Bunsenges. Phys. Chem. **102**, 745–750 (1998).

[5]M. Steinhart, M. Kriechbaum, K. Pressl *et al.*, "High-pressure instrument for small- and wide-angle x-ray scattering. II. Time-resolved experiments," Rev. Sci. Instrum. **70**, 1540–1545 (1999).

[6]J. Woenckhaus, R. Köhling, R. Winter *et al.*, "High pressure-jump apparatus for kinetic studies of protein folding reactions using the small-angle synchrotron x-ray scattering technique," Rev. Sci. Instrum. **71**, 3895–3899 (2000).

[7]J. Woenckhaus, R. Köhling, P. Thiyagarajan *et al.*, "Pressure-jump small-angle x-ray scattering detected kinetics of staphylococcal nuclease folding," Biophys. J. **80**, 1518–1523 (2001).

[8]H. Herberhold and R. Winter, "Temperature- and pressure-induced unfolding and refolding of ubiquitin: A static and kinetic Fourier transform infrared spectroscopy study," Biochemistry **41**, 2396–2401 (2002).

[9]H. Herberhold, S. Marchal, R. Lange *et al.*, "Characterization of the pressure-induced intermediate and unfolded state of red-shifted green fluorescent protein—A static and kinetic FTIR, UV/VIS and fluorescence spectroscopy study," J. Mol. Biol. **330**, 1153–1164 (2003).

[10]W. J. Evans, C.-S. Yoo, G. W. Lee *et al.*, "Dynamic diamond anvil cell (dDAC): A novel device for studying the dynamic-pressure properties of materials," Rev. Sci. Instrum. **78**, 073904 (2007).

[11]G. W. Lee, W. J. Evans, and C.-S. Yoo, "Crystallization of water in a dynamic diamond-anvil cell: Evidence for ice VII-like local order in supercompressed water," Phys. Rev. B **74**, 134112 (2006).

[12]J.-Y. Chen and C.-S. Yoo, "High density amorphous ice at room temperature," Proc. Natl. Acad. Sci. U. S. A. **108**, 7685–7688 (2011).

[13]G. W. Lee, W. J. Evans, and C.-S. Yoo, "Dynamic pressure-induced dendritic and shock crystal growth of ice VI," Proc. Natl. Acad. Sci. U. S. A. **104**, 9178–9181 (2007).

[14]S. V. Sinogeikin, J. S. Smith, E. Rod *et al.*, "Online remote control systems for static and dynamic compression and decompression using diamond anvil cells," Rev. Sci. Instrum. **86**, 072209 (2015).

[15]Y.-J. Kim, Y.-H. Lee, S. Lee *et al.*, "Shock growth of ice crystal near equilibrium melting pressure under dynamic compression," Proc. Natl. Acad. Sci. U. S. A. **116**, 8679–8684 (2019).

[16]H.-P. Liermann, W. Morgenroth, A. Ehnes *et al.*, "The Extreme conditions beamline at PETRA III, DESY: Possibilities to conduct time resolved monochromatic diffraction experiments in dynamic and laser heated DAC," J. Phys.: Conf. Ser. **215**, 012029 (2010).

[17]C. Lin, J. S. Smith, S. V. Sinogeikin *et al.*, "Experimental evidence of low-density liquid water upon rapid decompression," Proc. Natl. Acad. Sci. U. S. A. **115**, 2010–2015 (2018).
[18]C. Lin, J. S. Smith, S. V. Sinogeikin *et al.*, "A metastable liquid melted from a crystalline solid under decompression," Nat. Commun **8**, 1–6 (2017).
[19]B. Haberl, M. Guthrie, B. D. Malone *et al.*, "Controlled formation of metastable germanium polymorphs," Phys. Rev. B **89**, 144111 (2014).
[20]C. Lin, J. S. Smith, S. V. Sinogeikin *et al.*, "Kinetics of the B1-B2 phase transition in KCl under rapid compression," J. Appl. Phys. **119**, 045902 (2016).
[21]C. Lin, X. Yong, J. S. Tse *et al.*, "Kinetically controlled two-step amorphization and amorphous-amorphous transition in ice," Phys. Rev. Lett. **119**, 135701 (2017).
[22]H. Cheng, J. Zhang, Y. Li *et al.*, "A convenient dynamic loading device for studying kinetics of phase transitions and metastable phases using symmetric diamond anvil cells," High Pressure Res. **38**, 32–40 (2018).
[23]X. Dou, K. Ding, and B. Sun, "Development and application of piezoelectric driving diamond anvil cell device," Rev. Sci. Instrum. **88**, 123105 (2017).
[24]X. Wu, X. Dou, K. Ding *et al.*, "*In situ* tuning the single photon emission from single quantum dots through hydrostatic pressure," Appl. Phys. Lett. **103**, 252108 (2013).
[25]S. Yang, K. Ding, X. Dou *et al.*, "Zinc-blende and wurtzite GaAs quantum dots in nanowires studied using hydrostatic pressure," Phys. Rev. B **92**, 165315 (2015).
[26]Y. Ye, X. Dou, K. Ding *et al.*, "Single photon emission from deep-level defects in monolayer WSe_2," Phys. Rev. B **95**, 245313 (2017).
[27]L. Zhang, K. Shi, Y. Wang *et al.*, "Compression rate-dependent crystallization of pyridine," J. Phys. Chem. C **125**, 6983–6989 (2021).
[28]P. Xiong and M. Peng, "Near infrared mechanoluminescence from the Nd^{3+} doped perovskite $LiNbO_3$:Nd^{3+} for stress sensors," J. Mater. Chem. C **7**, 6301–6307 (2019).
[29]Y. Du, Y. Jiang, T. Sun *et al.*, "Mechanically excited multicolor luminescence in lanthanide ions," Adv. Mater. **31**, 1807062 (2019).
[30]C. G. Camara, J. V. Escobar, J. R. Hird *et al.*, "Correlation between nanosecond X-ray flashes and stick-slip friction in peeling tape," Nature **455**, 1089–1092 (2008).
[31]H. Zhang, Y. Wei, X. Huang *et al.*, "Recent development of elastico-mechanoluminescent phosphors," J. Lumin. **207**, 137–148 (2019).
[32]L. Zhang, K. Shi, Y. Wang *et al.*, "Unraveling the anomalous mechanoluminescence intensity change and pressure-induced red-shift for manganese-doped zinc sulfide," Nano Energy **85**, 106005 (2021).
[33]X. Wang, H. Zhang, R. Yu *et al.*, "Dynamic pressure mapping of personalized handwriting by a flexible sensor matrix based on the mechanoluminescence process," Adv. Mater. **27**, 2324–2331 (2015).